A morphology-independent search for gravitational wave echoes in data from the first and second observing runs of Advanced LIGO and Advanced Virgo

Ka Wa Tsang,[1,2,3] Archisman Ghosh,[1,4,5,6] Anuradha Samajdar,[1,3] Katerina Chatziioannou,[7]
Simone Mastrogiovanni,[8] Michalis Agathos,[9] and Chris Van Den Broeck[1,3]

[1]*Nikhef—National Institute for Subatomic Physics,*
105 Science Park, 1098 XG Amsterdam, The Netherlands
[2]*Van Swinderen Institute for Particle Physics and Gravity, University of Groningen,*
Nijenborgh 4, 9747 AG Groningen, The Netherlands
[3]*Department of Physics, Utrecht University, Princetonplein 1, 3584 CC Utrecht, The Netherlands*
[4]*Delta Institute for Theoretical Physics, Science Park 904, 1090 GL Amsterdam, The Netherlands*
[5]*Lorentz Institute, Leiden University, PO Box 9506, 2300 RA Leiden, The Netherlands*
[6]*GRAPPA, University of Amsterdam, Science Park 904, 1098 XH Amsterdam, The Netherlands*
[7]*Center for Computational Astrophysics, Flatiron Institute, 162 5th Ave, New York, New York 10010, USA*
[8]*APC, AstroParticule et Cosmologie, Université Paris Diderot, CNRS/IN2P3, CEA/Irfu,*
Observatoire de Paris, Sorbonne Paris Cité, F-75205 Paris Cedex 13, France
[9]*Department of Applied Mathematics and Theoretical Physics, Centre for Mathematical Sciences,*
University of Cambridge, Wilberforce Road, Cambridge CB3 0WA, United Kingdom

Gravitational wave echoes have been proposed as a smoking-gun signature of exotic compact objects with near-horizon structure. Recently there have been observational claims that echoes are indeed present in stretches of data from Advanced LIGO and Advanced Virgo immediately following gravitational wave signals from presumed binary black hole mergers, as well as a binary neutron star merger. In this paper we deploy a morphology-independent search algorithm for echoes introduced by Tsang *et al.* [Phys. Rev. D **98**, 024023 (2018)], which (a) is able to accurately reconstruct a possible echoes signal with minimal assumptions about their morphology, and (b) computes Bayesian evidences for the hypotheses that the data contain a signal, an instrumental glitch, or just stationary, Gaussian noise. Here we apply this analysis method to all the significant events in the first Gravitational Wave Transient Catalog (GWTC-1), which comprises the signals from binary black hole and binary neutron star coalescences found during the first and second observing runs of Advanced LIGO and Advanced Virgo. In all cases, the ratios of evidences for signal versus noise and signal versus glitch do not rise above their respective "background distributions" obtained from detector noise, the smallest *p*-value being 3% (for event GW170823). Hence we find no statistically significant evidence for echoes in GWTC-1.

I. INTRODUCTION

Over the past several years, the twin Advanced LIGO observatories [1] have been detecting gravitational wave (GW) signals from coalescences of compact binary objects on a regular basis [2–6]. Meanwhile Advanced Virgo [7] has joined the global network of detectors, leading to further detections, including a binary neutron star inspiral [8]. In the first and second observing runs a total of 11 detections were made, which are summarized in Ref. [9]; the latter reference will be referred to as GWTC-1 (for Gravitational Wave Transient Catalog 1). (For other detection efforts, see Refs. [10–12].)

Thanks to these observations, general relativity has been subjected to a range of tests. For the first time we had access to the genuinely strong-field dynamics of the theory

[2,4,5,13,14]. The possible dispersion of gravitational waves was strongly constrained, leading to stringent upper bounds on the mass of the graviton and on local Lorentz invariance violations [5,13,14]. As a next step, we want to probe the nature of the compact objects themselves. Based on the available data, how certain can we be that the more massive compact objects that were observed were indeed the standard black holes of classical, vacuum general relativity? A variety of alternative objects ("black hole mimickers") have been proposed; see e.g., Ref. [15] for an overview. When such objects are part of a binary system that undergoes coalescence, anomalous effects associated with them can leave an imprint upon the observed gravitational wave signal, including tidal effects [16,17], dynamical friction as well as resonant excitations due to dark matter clouds surrounding the objects [18], violations

064012-1

of the no-hair conjecture [19,20], and finally through gravitational wave "echoes" that might follow a merger [21–24] (for critical discussions, see Refs. [25,26], and Refs. [27,28] for thorough reviews).

In this paper we will search for echoes. In the case of exotic compact objects that lack a horizon, ingoing gravitational waves (e.g., resulting from a merger) can reflect multiple times off effective radial potential barriers, with wave packets leaking out at set times and escaping to infinity. Given an exotic object with mass M and a horizon modification with typical length scale ℓ, the time between these echoes tends to be constant, and approximately equal to $\Delta t \simeq nM \log(M/\ell)$, where n is a factor that is determined by the nature of the object [22]. Setting ℓ equal to the Planck length, for the masses involved in the binary coalescences of GWTC-1 one can expect Δt to range from a few to a few hundred milliseconds.

In Refs. [29,30], searches for echoes were presented using template waveforms characterized by the above Δt, the arrival time of the first echo, a truncation time scale related to the shape of the echoes, a damping factor between successive echoes, and an overall amplitude. Since then, template-based search methods were developed based on Bayesian model selection [31,32], or using more sophisticated templates [33]. A potential drawback here is that echo waveforms have been explicitly calculated only for selected exotic objects under various assumptions [22,23], and even then only in an exploratory way [34]. Hence it is desirable to have a method to search for and characterize *generic* echoes, irrespective of their detailed morphology. A model-independent search for echoes was presented in Ref. [35], which searched for periodic peaks of equal amplitude in the cross-power spectrum of two detectors at integer multiples of $f_{\rm echo} = 1/\Delta t$. In Ref. [36] a search was performed by looking for coherent excess power in a succession of windows in time or frequency. In this paper we instead employ the framework developed in Ref. [37] based on the BayesWave algorithm [38,39] which can be used to not only detect but also reconstruct and characterize echo signals of an *a priori* unknown form. Because our method allows for structure in the individual echoes, we expect our algorithm to perform better in terms of detection as well.

In what follows, we first briefly recall the morphology-independent echoes search methodology explained in Ref. [37] (Sec. II), which is then applied to events from GWTC-1, with a discussion of the results (Sec. III). The conclusion will be that we find no statistically significant evidence for echoes in data from the first and second observing runs of Advanced LIGO and Advanced Virgo.

II. METHOD

The method we use was extensively described in Ref. [37]; here we only give an overview and then describe how it was applied to data from GWTC-1. We model the detector data **s** as

$$\mathbf{s} = \mathbf{R} * \mathbf{h} + \mathbf{g} + \mathbf{n_g}, \qquad (1)$$

where $\mathbf{R}$ is the response of the network to gravitational waves, $\mathbf{h}$ is the potential signal that is coherent across the detectors, $\mathbf{g}$ denotes possible instrumental transients or glitches, and $\mathbf{n_g}$ is a contribution from stationary, Gaussian noise. The signal $\mathbf{h}$ and the glitches $\mathbf{g}$ can both be decomposed in terms of a set of basis functions, and Bayesian evidences can be obtained for the hypotheses that either are present in the data. An important difference between signals and glitches is that the former will be present in the data of all the detectors in a coherent way (taking into account the different antenna responses), whereas the latter will manifest themselves incoherently. If the data contain a coherent signal, then typically a smaller number of basis functions will be needed to reconstruct it than to reconstruct incoherent glitches, so that the glitch model incurs an Occam penalty. At the same time, a reconstruction of the shape of the signal is obtained from the corresponding superposition of basis functions. For our purposes a natural choice for the basis functions is a "train" of sine-Gaussians. Individual sine-Gaussians are characterized by an amplitude A, a central frequency f_0, a damping time τ, and a reference phase ϕ_0; the train of sine-Gaussians as a whole also involves a central time t_0 of the first sine-Gaussian, a time Δt between successive sine-Gaussians, and in going from one sine-Gaussian to the next also a relative phase shift $\Delta\phi$, an amplitude damping factor γ, and a widening factor w. Although there is no expectation that real echoes signals would resemble any one of these "generalized wavelets," it is reasonable to assume that *superpositions* of them will be able to catch a wide variety of physical echoes waveforms and, if the first few echoes are sufficiently loud, provide an adequate reconstruction. Finally, the noise model $\mathbf{n_g}$ consists of colored Gaussian noise, the power spectral density of which is computed using a combination of smooth spline curves and a collection of Lorentzians to fit sharp spectral lines [39]. For each of the three models, the relevant parameter space is sampled over using a reversible jump Markov chain Monte Carlo algorithm, in which the number of generalized wavelets is also allowed to vary freely. Evidences for the three hypotheses are estimated through thermodynamic integration, yielding Bayes factors $B_{S/N}$ and $B_{S/G}$ for, respectively, the signal versus noise and signal versus glitch models [38]. This allows us to not only perform model selection, but also to reconstruct and characterize the signal. The algorithm is also applied to many stretches of detector noise, leading to a background distribution for $B_{S/N}$ and $B_{S/G}$ which can then be used to assess the statistical significance of potential echoes signals by obtaining p-values. (For more details, see Ref. [37].)

This is analogous to how the log-likelihood ratio for presence versus absence of a signal is used in searching for, and establishing the significance of, candidate binary coalescence events [40,41].

In analyzing the stretches of data immediately preceding the events in GWTC-1 (for background calculation) or immediately after them (to search for echoes), we need to choose priors. We take f_0 to be uniform in the interval [30, 1024] Hz (respectively the lower cutoff frequency and half the sampling rate of the analysis), and the quality factor $Q = 2\pi f_0 \tau \in [2, 40]$ uniformly, so that τ takes values roughly between 3×10^{-4} and 0.2 s, consistent with time scales set by the masses involved in the events. We let ϕ_0 be uniform in $[0, 2\pi]$. For the wavelet amplitude A we put in a prior such that signal-to-noise ratios (SNRs) for individual wavelets have a distribution that smoothly goes to zero for SNR $\rightarrow 0$ as well as SNR $\rightarrow \infty$; this avoids large numbers of low-amplitude wavelets from being included in the reconstruction [38]. We take uniform priors $\Delta t \in [0, 0.7]$ s, $\Delta \phi \in [0, 2\pi]$, $\gamma \in [0, 1]$, and $w \in [1, 2]$. For definiteness, each generalized wavelet contains five sine-Gaussians. We also need to specify a prior for the central time of the first sine-Gaussian in a generalized wavelet. Here we want to start analyzing at a time that is safely beyond the plausible duration of the ringdown of the remnant object. Let t_{event} be the arrival time for a given binary coalescence event as given in Ref. [9]; then we take t_0 to be uniform in $[t_{event} + 4\tau_{220}, t_{event} + 4\tau_{220} + 0.5 \text{ s}]$. The value for τ_{220} is a conservatively long estimate for the decay time of the 220 mode in the ringdown, using the fitting formula $\tau_{220}(M_f, a_f, z)$ of Ref. [42], where for the final mass M_f, the final spin a_f, and the redshift z we take values at the upper bounds of the 90% confidence intervals listed in Ref. [9]; typically this amounts to a few milliseconds. We note that our choices for parameter prior ranges, though pertaining to generalized wavelet decompositions rather than waveform templates, include the corresponding values for t_0, γ, and A at which the template-based analysis of Ref. [29] claimed tentative evidence for echoes related to GW150914, GW151012, and GW151226.

We note that in existing gravitational wave data analysis implementations, the (log) Bayes factor can usually not be treated as a standalone, idealized quantity. Both in unmodeled searches [43,44] and in template-based inference [45], log Bayes factors tend to depend sensitively on the recovered SNR and can have relatively large values for SNRs that are below the detection threshold. For this reason, in our study, we do not use the Bayes factors computed from the data as the final products. Instead we factor in the "prior odds" to help normalize these Bayes factor values. Following common practice, we compare our foreground values of $\log B_{S/N}$ and $\log B_{S/G}$ to their respective background distributions, effectively introducing such "prior odds" [40,41,46]. To construct background

distributions we use stretches of data *preceding* each coalescence event in GWTC-1 in the following way. In the interval between 1050 and 250 s before the GPS time of a binary coalescence trigger as given in Ref. [9], we define 100 subintervals of 8 s each. (No signal in GWTC-1 will have been in the detectors' sensitive frequency band for more than 250 s; hence these intervals should effectively contain noise only.) For each of these intervals we compute $\log B_{S/N}$ and $\log B_{S/G}$, where the priors for the parameters of the generalized wavelets are as explained above; the values for t_{event} are chosen to be at the start of each interval. The log Bayes factors from times preceding all the events that were seen in two detectors obtained in this way are put into histograms, and the same is done separately for log Bayes factors from times preceding all the three-detector events. These histograms are normalized, and smoothened using Gaussian kernel density estimates to obtain approximate probability distributions for $\log B_{S/N}$ and $\log B_{S/G}$ in the absence of echoes signals.
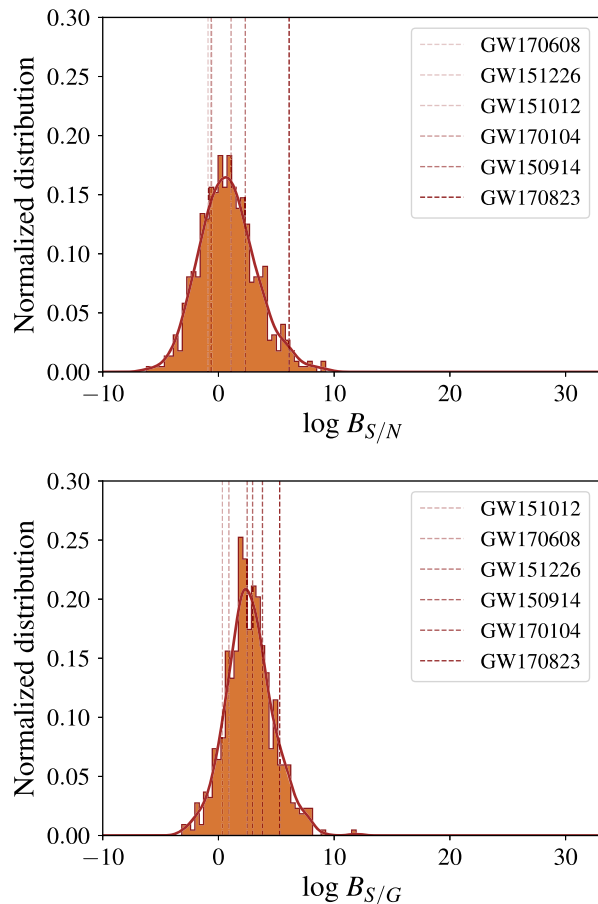

FIG. 1.   Background distributions (orange histograms, smoothened in brown) and foreground (vertical dashed lines, shaded by their values and labeled left to right) for the log Bayes factors for signal versus noise $\log B_{S/N}$ (top) and signal versus glitch $\log B_{S/G}$ (bottom), for the two-detector events of GWTC-1. The associated p-values can be found in Table I.
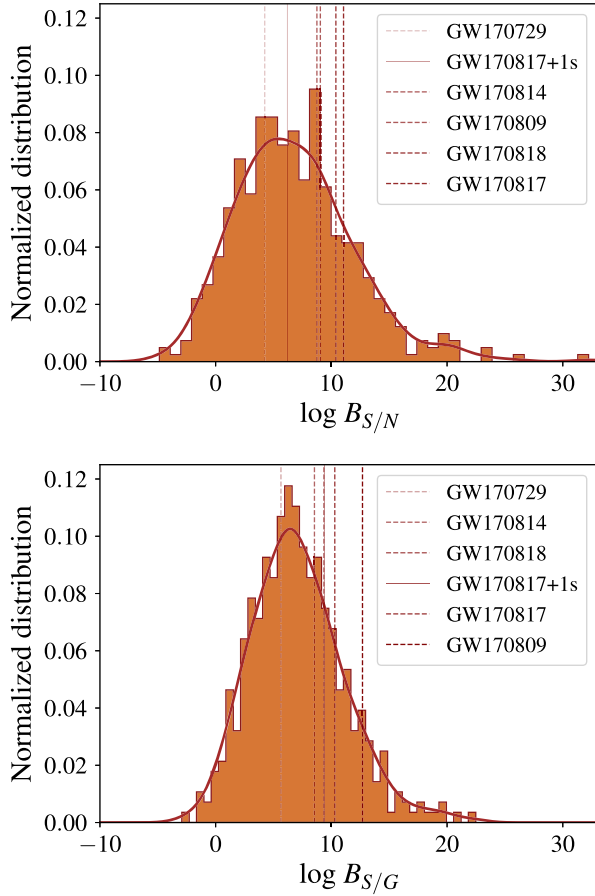
FIG. 2. The same as in Fig. 1, but now for the three-detector events of GWTC-1. The thin solid lines in each of the two panels are for an analysis of GW170817 in which the prior range for the time of the first echo was centered at 1.0 s after the event time, where Ref. [35] claimed tentative evidence for an echo. For the associated *p*-values, see Table II.

Finally, we calculate log Bayes factors for times *following* the coalescence events of GWTC-1, using the same priors, but now setting t_{event} to the arrival times for the events given in Ref. [9]. Considering $\log B_{S/N}$ or $\log B_{S/G}$ and the relevant number of detectors, the normalized, smoothened background distributions $\mathcal{P}(\log B)$ are used to compute *p*-values:

$$p = 1 - \int_{-\infty}^{\log B} \mathcal{P}(x)dx. \qquad (2)$$

Combined *p*-values from all the events are obtained using Fisher's prescription [47]. Given individual *p*-values p_i, $i = 1, \ldots, N$, one defines

$$S = -2 \sum_{i=1}^{N} \log(p_i), \qquad (3)$$

and the combined *p*-value is calculated as

TABLE I. Log Bayes factors for signal versus noise and signal versus glitch, and the corresponding *p*-values, for events seen in two detectors. The bottom row contains the combined *p*-values for all these events together.

Event	$\log B_{S/N}$	$p_{S/N}$	$\log B_{S/G}$	$p_{S/G}$
GW150914	2.32	0.26	2.95	0.43
GW151012	−0.59	0.70	0.35	0.88
GW151226	−0.67	0.72	2.48	0.53
GW170104	1.09	0.44	3.80	0.28
GW170608	−0.90	0.75	0.90	0.82
GW170823	6.11	0.03	5.29	0.11
Combined		0.34		0.57

$$p_{\text{comb}} = 1 - \int_0^S \chi_{2N}^2(x)dx, \qquad (4)$$

where χ_{2N}^2 is the chi-squared distribution with $2N$ degrees of freedom.

III. RESULTS AND DISCUSSION

Figures 1 and 2 show background and foreground for $\log B_{S/N}$ and $\log B_{S/G}$ in the case of, respectively, two-detector and three-detector signals, and in Tables I and II we list the specific log Bayes factors for these cases, as well as associated *p*-values. As expected from the prior on SNR, which peaks away from zero, the distributions of log Bayes factors tend to peak at positive values. In the case of the signal hypothesis, the wavelet SNRs will moreover increase with the number of antenna pattern functions that are folded in, so that the effect is more visible in the three-detector case [38]. Note also how both the $\log B_{S/N}$ and the $\log B_{S/G}$ background distributions have support for large and positive values, which is not surprising. As mentioned earlier, in practice log Bayes factors usually depend sensitively on the recovered SNR and can have relatively large values also for SNRs below the detection threshold. In particular, $\log B_{S/N}$ generically scales as $\log B_{S/N} \sim (1/2)\text{SNR}^2$ in

TABLE II. The same as in Table II, but now for the events that were seen in three detectors. In the case of GW170817 we also include results for which the prior range for the time of the first echo was centered at 1.0 s after the event time, where Ref. [35] claimed tentative evidence for an echo. The combined *p*-values take the latter prior choice for this particular event.

Event	$\log B_{S/N}$	$p_{S/N}$	$\log B_{S/G}$	$p_{S/G}$
GW170729	4.24	0.67	5.64	0.62
GW170809	9.05	0.31	12.69	0.09
GW170814	8.75	0.33	8.54	0.34
GW170817	11.05	0.19	10.30	0.20
GW170817 + 1s	6.19	0.52	9.39	0.27
GW170818	10.39	0.23	9.36	0.27
Combined		0.47		0.22

unmodeled searches [43,44] and in template-based inference [45] alike. In the particular case of BayesWave and the assessment of signal versus glitches one has $\log B_{S/G} \sim N \log \mathrm{SNR}$, where N is the number of wavelets used [43,44]. As a consequence, even a recovered SNR below detection threshold (which is usually around 8–10 [37]) can result in large values of the Bayes factors. Also note how this effect is larger in the three-detector case; this is because BayesWave is configured to expect the SNR to increase

with the number of detectors, which further increases the sensitivity of log Bayes factors to the SNR, and the fact that the Virgo detector tends to be less quiet than the two LIGO detectors. (In this regard, see Fig. 1 of Ref. [48] and the surrounding discussion.)

All foreground results are in the support of the relevant background distributions. For signal versus noise, the smallest p-value is 3% (the case of GW170823), whereas for signal versus glitch the p-values do not go below 9%
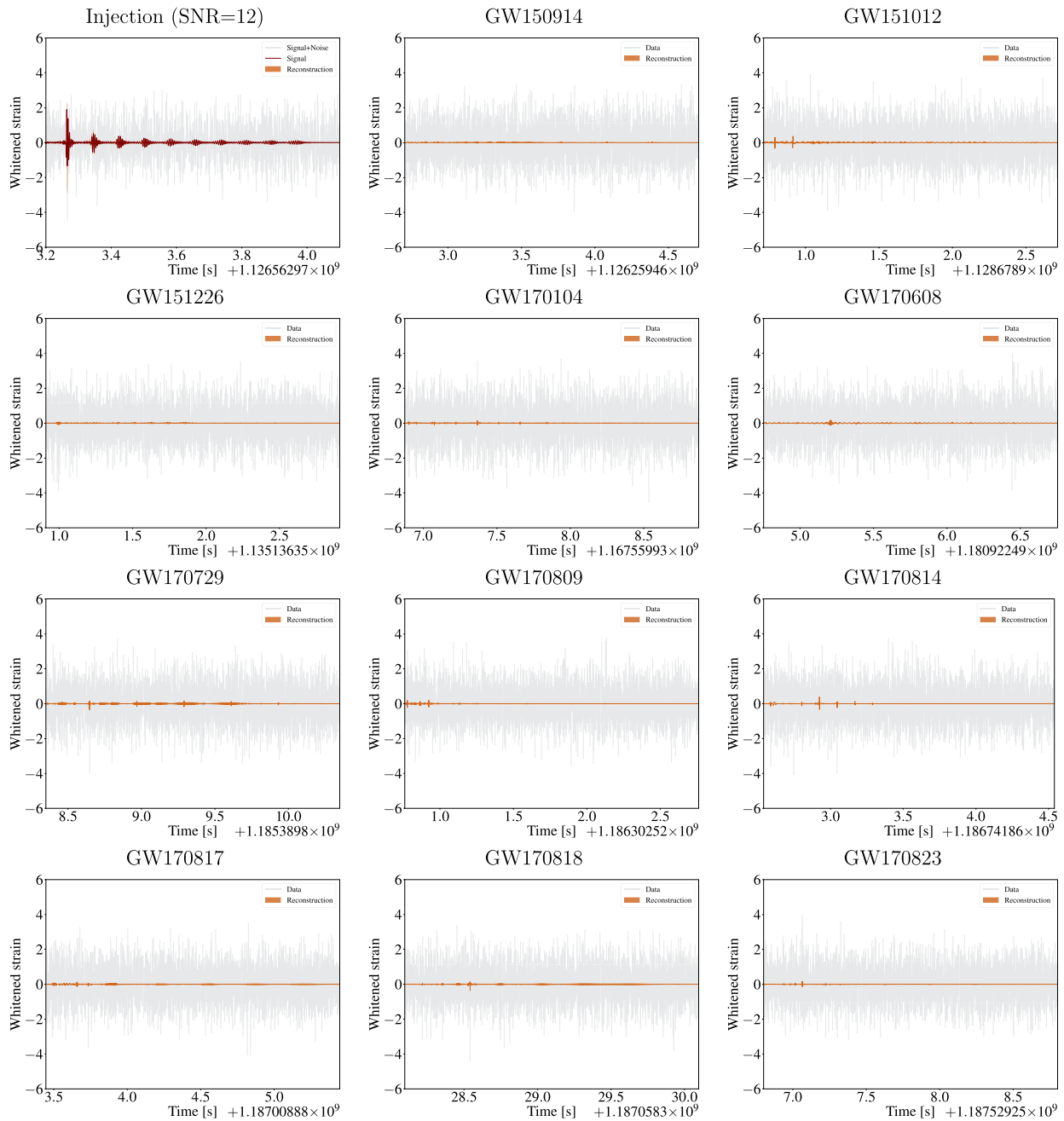

FIG. 3. Stretches of whitened data (gray) and signal reconstructions (red) for a simulated echoes signal as described in the main text (top left panel) and for data immediately after the events in GWTC-1. In the case of GW170817, the first echo is searched for in an interval centered at 1.0 s after the event time. In all cases the event GPS time corresponds to the left bound of the panel.

(see GW170809). In summary, we find no statistically significant evidence for echoes in GWTC-1. For the binary black hole observations in particular, this statement is in agreement with the template-based searches in Refs. [30,32,33]. (Note that a *quantitative* comparison of p-values is hard to make, because of the very specific signal shapes that were assumed in the latter analyses.)

Our results in Fig. 2 and Table II include the binary neutron star inspiral GW170817, analyzed in the same manner as the binary black hole merger signals. In Ref. [49], an analysis using the original BayesWave algorithm of Refs. [38,39] (i.e., employing wavelets that are simple sine-Gaussians) yielded no evidence for a post-merger signal. Using our generalized wavelets, we obtain $\log B_{S/N} = 11.05$ and $\log B_{S/G} = 10.30$, both consistent with background. Hence in particular we do not find evidence for an echoes-like post-merger signal either, at least not up to $\lesssim 0.5$ s after the event's GPS time. In Ref. [35], tentative evidence was claimed for echoes starting at $t_0 = t_{\text{event}} + 1.0$ s. Reanalyzing with the same priors as above but this time with $t_0 \in [t_{\text{event}} + 0.75$ s, $t_{\text{event}} + 1.25$ s], we find $\log B_{S/N} = 6.19$ and $\log B_{S/G} = 9.39$, both of which are consistent with their respective background distributions. Hence also when the time of the first echo is in this time interval we find no significant evidence for echoes. That said, we explicitly note that in the case of a black hole resulting from a binary neutron star merger of total mass $\sim 2.7\, M_\odot$ [49], we expect the dominant ringdown frequency and hence the central frequency f_0 of the echoes to be above 6000 Hz, i.e., above our prior upper bound, but also much beyond the detectors' frequency reach for plausible energies emitted [50]. Foreground and background analyses with a correspondingly high frequency range are left for future work.

Our nonobservation of echoes can be used to put a (weak) upper limit on the reflectivity $\mathcal{R}$, under the assumption that the remnant objects of GWTC-1 were exotic compact objects after all. Following Ref. [51] and given that the GWTC-1 event with the highest signal-to-noise ratio in ringdown (namely GW150914) had $\rho_{\text{ringdown}} \sim 8.5$ [13], our nonobservation of echoes leads to $\mathcal{R} \lesssim 0.998$ at 4σ confidence.

Finally, in Fig. 3 we show signal reconstructions (medians and 90% credible intervals) in terms of generalized wavelets for all the GWTC-1 events. For illustration purposes we also include the reconstruction of a simulated echoes waveform following the inspiral of a particle in a Schwarzschild spacetime with Neumann reflective boundary conditions just outside of where the horizon would have been, at mass ratio $q = 100$ [52,53]. The simulated signal was embedded into detector noise at a SNR of 12, roughly corresponding to the SNR in the ringdown part of GW150914, had it been observed with Advanced LIGO sensitivity of the second observing run. In all cases the whitened raw data is shown, along with the whitened signal reconstruction. We include these reconstructions for completeness; our main results are the ones in Figs. 1 and 2 and Tables I and II. Nevertheless, the reconstruction plots are visually consistent with our core results.

ACKNOWLEDGMENTS

[1] J. Aasi *et al.* (LIGO Scientific Collaboration), Classical Quantum Gravity **32,** 074001 (2015).

[2] B. P. Abbott *et al.* (LIGO Scientific and Virgo Collaborations), Phys. Rev. Lett. **116,** 061102 (2016).

[3] B. P. Abbott *et al.* (LIGO Scientific and Virgo Collaborations), Phys. Rev. Lett. **116,** 241103 (2016).

[4] B. P. Abbott *et al.* (LIGO Scientific and Virgo Collaborations), Phys. Rev. X **6,** 041015 (2016).

[5] B. P. Abbott *et al.* (LIGO Scientific and Virgo Collaborations), Phys. Rev. Lett. **118,** 221101 (2017).

[6] B. P. Abbott *et al.* (LIGO Scientific and Virgo Collaborations), Astrophys. J. **851,** L35 (2017).

[7] F. Acernese *et al.* (Virgo Collaboration), Classical Quantum Gravity **32,** 024001 (2015).

[8] B. P. Abbott *et al.* (LIGO Scientific and Virgo Collaborations), Phys. Rev. Lett. **119,** 161101 (2017).

[9] B. P. Abbott *et al.* (LIGO Scientific and Virgo Collaborations), Phys. Rev. X **9,** 031040 (2019).

[10] A. H. Nitz, C. Capano, A. B. Nielsen, S. Reyes, R. White, D. A. Brown, and B. Krishnan, Astrophys. J. **872,** 195 (2019).

[11] T. Venumadhav, B. Zackay, J. Roulet, L. Dai, and M. Zaldarriaga, Phys. Rev. D **100,** 023011 (2019).

[12] T. Venumadhav, B. Zackay, J. Roulet, L. Dai, and M. Zaldarriaga, arXiv:1904.07214.

[13] B. P. Abbott *et al.* (LIGO Scientific and Virgo Collaborations), Phys. Rev. Lett. **116,** 221101 (2016).

[14] B. P. Abbott *et al.* (LIGO Scientific and Virgo Collaborations), Phys. Rev. Lett. **123,** 011102 (2019).

[15] L. Barack *et al.*, Classical Quantum Gravity **36**, 143001 (2019).

[16] V. Cardoso, E. Franzin, A. Maselli, P. Pani, and G. Raposo, Phys. Rev. D **95**, 084014 (2017); **95**, 089901(A) (2017).

[17] N. K. Johnson-Mcdaniel, A. Mukherjee, R. Kashyap, P. Ajith, W. Del Pozzo, and S. Vitale, arXiv:1804.08026.

[18] D. Baumann, H. S. Chia, and R. A. Porto, Phys. Rev. D **99**, 044001 (2019).

[19] G. Carullo *et al.*, Phys. Rev. D **98**, 104020 (2018).

[20] R. Brito, A. Buonanno, and V. Raymond, Phys. Rev. D **98**, 084038 (2018).

[21] V. Cardoso, E. Franzin, and P. Pani, Phys. Rev. Lett. **116**, 171101 (2016); **117**, 089902(E) (2016).

[22] V. Cardoso, S. Hopper, C. F. B. Macedo, C. Palenzuela, and P. Pani, Phys. Rev. D **94**, 084031 (2016).

[23] V. Cardoso and P. Pani, Nat. Astron. **1**, 586 (2017).

[24] V. Cardoso, V. F. Foit, and M. Kleban, J. Cosmol. Astropart. Phys. 08 (2019) 006.

[25] B. Chen, Y. Chen, Y. Ma, K.-L. R. Lo, and L. Sun, arXiv:1902.08180.

[26] A. Addazi, A. Marcianò, and N. Yunes, Eur. Phys. J. C **80**, 36 (2020).

[27] V. Cardoso and P. Pani, Nat. Astron. **1**, 586 (2017).

[28] V. Cardoso and P. Pani, Living Rev. Relativity **22**, 4 (2019).

[29] J. Abedi, H. Dykaar, and N. Afshordi, Phys. Rev. D **96**, 082004 (2017).

[30] J. Westerweck, A. Nielsen, O. Fischer-Birnholtz, M. Cabero, C. Capano, T. Dent, B. Krishnan, G. Meadors, and A. H. Nitz, Phys. Rev. D **97**, 124037 (2018).

[31] R. K. L. Lo, T. G. F. Li, and A. J. Weinstein, Phys. Rev. D **99**, 084052 (2019).

[32] A. B. Nielsen, C. D. Capano, O. Birnholtz, and J. Westerweck, Phys. Rev. D **99**, 104012 (2019).

[33] N. Uchikata, H. Nakano, T. Narikawa, N. Sago, H. Tagoshi, and T. Tanaka, Phys. Rev. D **100**, 062006 (2019).

[34] Z. Mark, A. Zimmerman, S. M. Du, and Y. Chen, Phys. Rev. D **96**, 084002 (2017).

[35] J. Abedi and N. Afshordi, J. Cosmol. Astropart. Phys. 11 (2019) 010.

[36] R. S. Conklin, B. Holdom, and J. Ren, Phys. Rev. D **98**, 044021 (2018).

[37] K. W. Tsang, M. Rollier, A. Ghosh, A. Samajdar, M. Agathos, K. Chatziioannou, V. Cardoso, G. Khanna, and C. Van Den Broeck, Phys. Rev. D **98**, 024023 (2018).

[38] N. J. Cornish and T. B. Littenberg, Classical Quantum Gravity **32**, 135012 (2015).

[39] T. B. Littenberg and N. J. Cornish, Phys. Rev. D **91**, 084034 (2015).

[40] S. Sachdev *et al.*, arXiv:1901.08580.

[41] B. P. Abbott *et al.* (LIGO Scientific and Virgo Collaborations), Phys. Rev. D **100**, 024017 (2019).

[42] E. Berti, V. Cardoso, and C. M. Will, Phys. Rev. D **73**, 064030 (2006).

[43] T. B. Littenberg, J. B. Kanner, N. J. Cornish, and M. Millhouse, Phys. Rev. D **94**, 044050 (2016).

[44] J. B. Kanner, T. B. Littenberg, N. Cornish, M. Millhouse, E. Xhakaj, F. Salemi, M. Drago, G. Vedovato, and S. Klimenko, Phys. Rev. D **93**, 022002 (2016).

[45] J. Veitch and A. Vecchio, Classical Quantum Gravity **25**, 184010 (2008).

[46] M. Isi, R. Smith, S. Vitale, T. J. Massinger, J. Kanner, and A. Vajpeyi, Phys. Rev. D **98**, 042007 (2018).

[47] R. A. Fisher, *Statistical Methods for Research Workers*, 14th revised ed. (Oliver and Boyd, 1970).

[48] B. P. Abbott *et al.* (LIGO Scientific and Virgo Collaborations), Phys. Rev. D **100**, 104036 (2019).

[49] B. P. Abbott *et al.* (LIGO Scientific and Virgo Collaborations), Phys. Rev. X **9**, 011001 (2019).

[50] B. P. Abbott *et al.* (LIGO Scientific and Virgo Collaborations), Astrophys. J. **851**, L16 (2017).

[51] A. Testa and P. Pani, Phys. Rev. D **98**, 044018 (2018).

[52] G. Khanna and R. H. Price, Phys. Rev. D **95**, 081501 (2017).

[53] R. H. Price and G. Khanna, Classical Quantum Gravity **34**, 225005 (2017).